Large-Scale Circulation Anomalies and Intraseasonal Oscillations Associated with Long-Lived Extreme Heat Events in South China

RUIDAN CHEN

Center for Monsoon and Environment Research, and Guangdong Province Key Laboratory for Climate Change and Natural Disaster Studies, School of Atmospheric Sciences, Sun Yat-sen University, Guangzhou, and State Key Laboratory of Numerical Modeling for Atmospheric Sciences and Geophysical Fluid Dynamics, Institute of Atmospheric Physics, Chinese Academy of Sciences, Beijing, and Jiangsu Collaborative Innovation Center for Climate Change, Nanjing, China

ZHIPING WEN

Institute of Atmospheric Sciences, Fudan University, Shanghai, and Jiangsu Collaborative Innovation Center for Climate Change, Nanjing, China

RIYU LU

State Key Laboratory of Numerical Modeling for Atmospheric Sciences and Geophysical Fluid Dynamics, Institute of Atmospheric Physics, Chinese Academy of Sciences, and University of the Chinese Academy of Sciences, Beijing, China

(Manuscript received 10 April 2017, in final form 26 September 2017)

ABSTRACT

South China experiences extreme heat (EH) most frequently in eastern China. This study specifically explores the large-scale circulation anomalies associated with long-lived EH events in south China. The results show that there is an anomalous cyclone (anticyclone) and active (inactive) convection over south China (the western Pacific) before the EH onset; then, an anticyclone develops and moves northwestward and dominates over south China on the onset day. The anomalous anticyclone maintains its strength over south China and then diminishes and is replaced by another cyclone migrating from the western Pacific after the final day of the EH event. Consequently, the temperature increases over south China around the onset day and is anomalously warm for approximately 10 days on average and then decreases shortly thereafter. The fluctuating anomalies over south China and the western Pacific are intimately related to two intraseasonal oscillation (ISO) modes, namely, the 5–25- and 30–90-day oscillations, which originate from the tropical western Pacific and propagate northwestward. The 5–25-day oscillation is vital to triggering and terminating EH, accounting for approximately half of the original temperature and circulation anomaly transitions. The 30–90-day oscillation favors the persistent warming during EH events, accounting for approximately one-third of the original prolonged warming and anticyclonic anomaly. This result suggests that different ISO modes play crucial roles at different stages of the events. Moreover, a higher annual frequency of long-lived EH days in south China is associated with the transition phase from El Niño to La Niña. It is suggested that both medium-range and interannual forecasting of long-lived EH in south China are possible.

1. Introduction

Against the background of global warming, the surface air temperature is undergoing a sustained warming trend (Collins et al. 2000; Alexander et al. 2006; Li and Yan 2009; Wei and Chen 2011; WMO 2013). The latest World Meteorological Organization (WMO) report on global climate stated that 2011–15 was the warmest 5-yr period on record, with unprecedented warming widespread across every continent except Africa (WMO 2015). In July 2015, western and central Europe experienced the most severe heat wave since the deadly heat wave in 2003. A persistent heat wave swept many parts of eastern Asia (such as Japan, South Korea, and eastern China) in July and August 2013, with a peak temperature of 41.6°C occurring in Hangzhou, a city located in

Corresponding author: Ruidan Chen, chenrd3@mail.sysu.edu.cn

DOI: 10.1175/JCLI-D-17-0232.1

eastern China. The persistent occurrence of extreme heat (EH) greatly threatens human health and causes substantial economic losses (Teofilo and Stitt 1995; Kilbourne 1997; Valor et al. 2001; Coumou and Rahmstorf 2012). For instance, more than 3700 deaths in India and Pakistan resulted from the heat wave in May and June 2015 (WMO 2015). Approximately 1%–3% of the available daytime work hours were estimated to have been lost as a result of EH by the mid-1990s, significantly reducing productivity and economic output (UNDP 2016). Moreover, the frequency of EH events and the subsequent impacts on humans and society are projected to increase (Kunkel et al. 2010; Lau and Nath 2012; IPCC 2013; Li et al. 2014; Lelieveld et al. 2016; UNDP 2016). Therefore, there is undoubtedly an urgent demand to understand the causes of EH.

South China is located in a tropical–subtropical region and is influenced by the East Asian southwesterly monsoon in the summer. South China has also witnessed an obvious increasing trend of EH frequency in recent decades (~4.5 days decade^{-1}), ranking high among the different regions in eastern China (Gao et al. 2008; Wei and Chen 2009; Wang et al. 2016). In addition, south China is densely populated, making it more vulnerable to EH in terms of societal impacts. For example, Guangdong Province, located in south China, has a population of over 100 million and is growing at a rate of 1.9% yr^{-1}. Hence, investigating the causes of EH in south China is of great significance to social development.

The large-scale circulations responsible for the occurrence of EH in south China exhibit unique features. Typically, the occurrence of EH is caused by an anticyclonic anomaly over the high-temperature region, which induces more adiabatic heating, reduces cloud cover, and increases solar radiation at the surface (Black et al. 2004; Wei et al. 2004; Gershunov et al. 2009; Zhang and Zhang 2010; Fang and Jian 2011). However, our prior work found that the composite circulation pattern associated with EH in south China is different from the typical anticyclonic pattern and is uniquely characterized by a pair of anticyclonic–cyclonic anomalies in the lower troposphere (Chen and Lu 2015). According to this work, there is an anomalous anticyclone over south China and an anomalous cyclone to the southeast of south China. This finding points to the scientific significance of determining what causes EH in south China.

The boreal summer intraseasonal oscillation (ISO) over the western Pacific is considered a key factor that influences the variation of climate in East Asia, and two predominant ISO bands lie at 5–25-day (also refers to the 10–20- or 10–25-day bands in some references) and 30–90-day (also refers to the 30–60- or 25–90-day bands in some references) time scales (Ren and Huang 2002; Mao and Chan 2005; Chen et al. 2015). The 5–25- and 30–90-day oscillations originate from the equatorial Pacific and propagate either northwestward or northward, modulating the subtropical monsoon flow and subsequently the climate over East Asia, including south China (Jia and Yang 2013; Xu and Lu 2015; Chen and Zhai 2017; Gao et al. 2017). During the ISO life cycle, the dominance of the anticyclonic phase induces anomalous subsidence and drier air conditions, favoring higher temperatures and the occurrence of EH events. In contrast, the appearance of the cyclonic phase decreases the air temperature and inhibits EH events. Therefore, the duration of EH events might be related to the periodicity of the dominant ISO.

In our prior work, Chen et al. (2016), we suggested that the 5–25-day oscillation of the tropical atmosphere plays a vital role in the occurrence of EH events over south China and that the warming related to the 5–25-day oscillation accounts for 80% of the warming amplitude on the day of EH onset. Consistent with the 5–25-day oscillation, the higher temperature lasts for about three days after the onset of an EH event in the composite results of Chen et al. (2016; their Fig. 7), which is approximately equal to ¼ of the 5–25-day ISO periodicity. A preliminary survey on the duration of the EH events defined by Chen et al. (2016) shows that 63% of the events last for no more than three days, as illustrated in Fig. 1a.

However, the EH events in south China can last for much longer. For example, in the summer of 2003, a record-breaking heat wave hit south China, with a large area suffering from EH for more than 1 month (Wang et al. 2006). In July 2007, a severe heat wave swept across Guangdong Province, resulting in an average duration of EH of up to 14 days over all observational stations (Liu et al. 2008). Such extreme heat waves bring continuous severe heat conditions and inhibit humans from good rest, thus posing a greater threat to human society than short-lived EH events. Therefore, specific studies on long-lived EH events should be undertaken to understand the causes of their occurrence.

Several case studies have been conducted on long-lived EH events in south China. Yang and Li (2005) and Wang et al. (2016) analyzed the circulation characteristics during the EH event in 2003 and suggested that the prolonged abnormal strong and western-extending subtropical high was responsible for the occurrence of continuous EH in south China. Liu et al. (2008) analyzed the persistent EH event in Guangdong Province in July 2007 and obtained similar results. However, the results of these studies are based on analyses of limited cases, which are obviously different from the composite results of Chen et al. (2016) representing short-lived EH events,

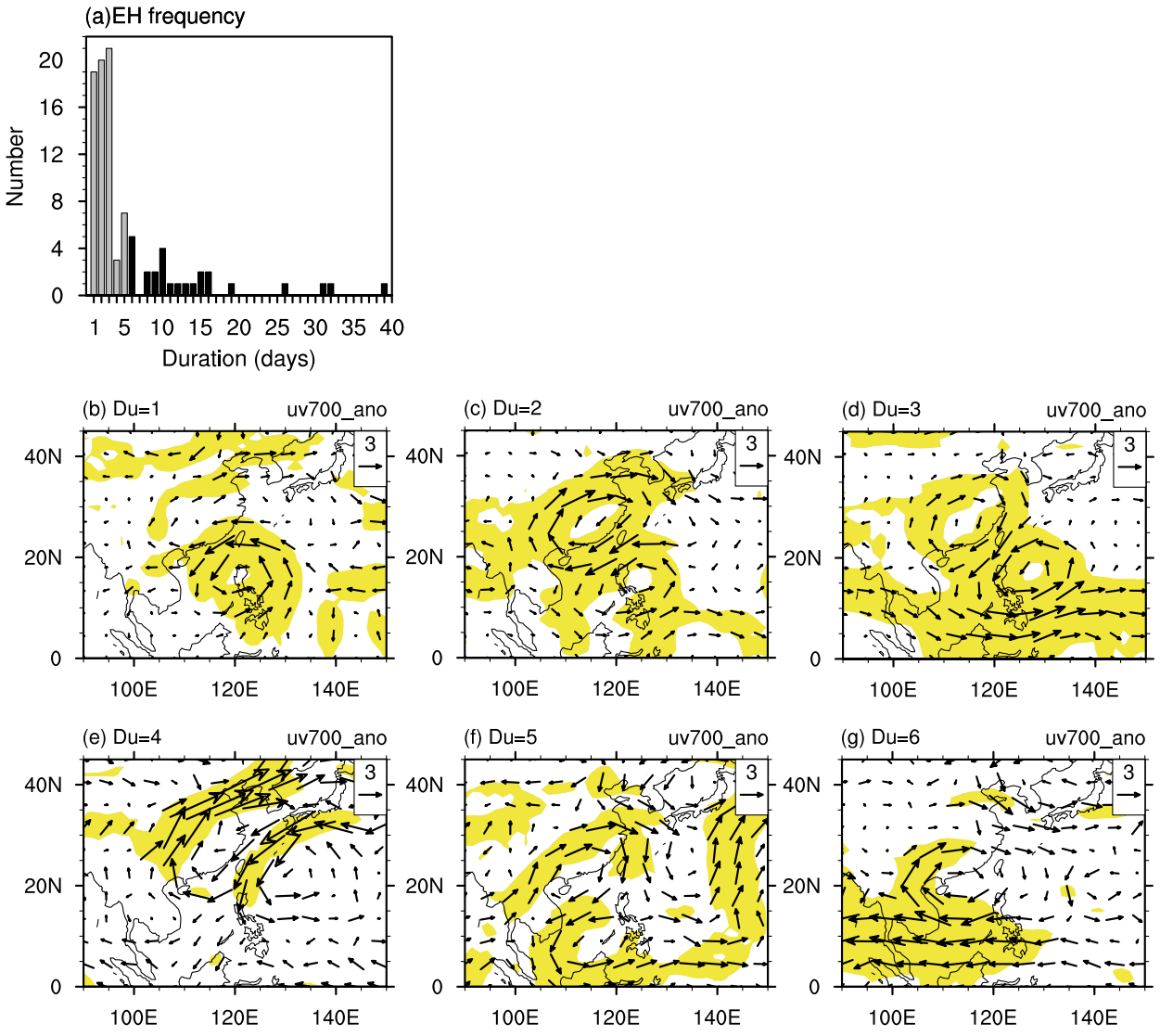

FIG. 1. (a) Occurrence frequency of EH events with different durations (days). Long-lived (black bars) and short-lived (gray bars) EH events lasting for more and less than 5 days, respectively. (b)–(g) Composite 700-hPa wind anomalies (vectors; m s^{-1}) averaged from −2 days to the onset day for the EH events with durations ranging from 1 to 6 days. The shaded areas indicate that either the zonal or meridional wind anomaly is significant at the 95% confidence level.

that is, the anticyclone–cyclone pair. The indication therefore is that the circulation patterns responsible for long-lived EH events might be distinct from those responsible for short-lived EH events. Investigating the large-scale circulation anomalies associated with long-lived EH events from a climatological viewpoint forms the primary motivation for this study. The roles of ISOs are addressed, including the 5–25- and 30–90-day oscillations.

On the other hand, the annual frequency of EH may be modulated by tropical sea surface temperature anomalies (SSTAs). El Niño–Southern Oscillation (ENSO), which is the most outstanding mode of the interannual variation of tropical Pacific SSTAs, is emphasized as an important factor influencing the East Asian climate. Previous studies have suggested that during the summer following the mature phase of El Niño, there is an anomalous anticyclone over the western North Pacific (Wang et al. 2000; Xie et al. 2009; Wu et al. 2010). The anomalous anticyclone might influence the temperature in south China and thus modulate the frequency of EH. The current study determines the influence of ENSO on the annual frequency of long-lived EH days in south China.

The remainder of the paper is organized as follows. Section 2 describes the data, definitions, and methods.

Section 3 presents the temporal and spatial evolutions of temperature anomalies associated with long-lived EH events in south China. Section 4 explores the large-scale circulation anomalies associated with long-lived EH events and the influences of ISOs. Section 5 further detects the influence of ENSO on the annual frequency of long-lived EH days in south China. Section 6 presents the conclusions of the study.

2. Data, definitions, and methods

a. Data

The data period is from July to August between 1979 and 2013. This selection of the summer season is the same as in Chen et al. (2016), in which it is indicated that EH days in July and August account for 89% of the total EH days in south China.

The data used in this study are extracted from four datasets. First, the daily temperature data are from the homogenized mean, maximum, and minimum surface air temperature series from 753 national standard stations in China (Li et al. 2016), which were revised to remove the inhomogeneity caused by frequent changes in observing locations and protocols (Li and Yan 2009). Second, the 6-hourly circulation data are from the European Centre for Medium-Range Weather Forecasts (ECMWF) interim reanalysis (ERA-Interim; Dee et al. 2011), with a horizontal resolution of 1.5° × 1.5° and 23 vertical pressure levels from 1000 to 200 hPa. The data at 0600 UTC (1400 local standard time) are used to represent the circulation associated with EH. Third, the daily outgoing longwave radiation (OLR) anomalies are derived from the National Oceanic and Atmospheric Administration (Liebmann and Smith 1996), which act as a proxy for anomalous large-scale convective activity. The horizontal resolution of the OLR data is 2.5° × 2.5°. Fourth, the monthly sea surface temperature data are derived from the HadISST, with a horizontal resolution of 1° × 1° (Rayner et al. 2003).

b. Definitions

The area of south China covered by this study includes the observational stations south of 28°N and east of 105°E, including 149 stations in total (denoted by the blue dots in Figs. 4 and 5). EH is defined as the days when more than one-third of the 149 stations in south China recorded a maximum temperature T_{max} above 35°C. The threshold of 35°C is adopted by the China Meteorological Administration to define EH and is widely used in various studies (e.g., Wei and Chen 2009; Chen and Lu 2014a,b). This definition yields a total of 436 EH days in south China, accounting for 20% of the study period (2170 days). Furthermore, EH days with gaps of no more than 5 days are merged into one EH event. Finally, 96 EH events are obtained, and the average duration of each event is 4.5 days. These definitions of south China EH and EH events are the same as in Chen et al. (2016). Another definition of EH, where both $T_{max} > 35$°C and minimum temperature $T_{min} > 25$°C, was also examined, and the results were similar to those presented in the current study (not shown).

The EH events are further divided into long- and short-lived EH events. To decide the division criterion, we first perform a general survey on the composite circulation anomalies responsible for EH events with different durations (1, 2, 3 days, and so on). It turns out that the composite circulation anomalies associated with EH events lasting no more than 5 days (1–5 days) are similar and are characterized by an anticyclone–cyclone pair around south China (Figs. 1b–f). In contrast, the circulation anomalies associated with EH events lasting for 6 days exhibit distinct patterns, featuring an anticyclone over south China (Fig. 1g). In addition, the longest EH event—that is, the 2003 EH event spanning 39 days from 4 July to 11 August (including 28 EH days satisfying our definition)—is also related to a persistent anticyclonic anomaly over south China (not shown). Thus, the circulation anomalies responsible for the occurrence of short- and long-lived EH events might be different, and EH events with duration >5 days (≤5 days) can be classified as long-lived (short lived) EH events.

According to the abovementioned definitions, there are a total of 26 long-lived EH events (including 274 EH days) and 70 short-lived EH events (including 162 EH days). The short-lived EH events account for the majority (73%) of all events; thus, the analysis results of the short-lived EH events are similar to the results of all events, as presented in Chen et al. (2016) (not shown). Therefore, the current study specifically focuses on the long-lived EH events, investigating the related large-scale characteristics and causes. Despite the lower proportion, long-lived EH events include 1.7 times as many EH days as the short-lived EH events, posing a greater threat and suggesting the importance for understanding the reasons for occurrence.

c. Methods

A composite analysis is performed to investigate the large-scale anomalies associated with long-lived EH events from a climatological perspective. The anomalies around both the EH onset day and end day are analyzed to comprehensively understand the entire process of long-lived EH events. When analyzing the spatial evolutions of large-scale anomalies, nonoverlapping 3-day means around the onset and end days (from −6

to −4 days, from −3 to −1 day, onset or end day, from +1 to +3 days, and from +4 to +6 days) are used to exclude synoptic variations, which are not the subject of this study. The daily anomalies are computed by deducting the climatology of the corresponding days from the raw data. The Student's *t* test with a confidence level of 95% and effective sample lengths is used to estimate the temporal significance of the composite anomalies (Wilks 2006).

Field significance testing is further performed on each composite field, based on the Monte Carlo techniques proposed by Livezey and Chen (1983). First, 1000 random simulations are carried out to select 26 days (representing the onset days of 26 long-lived EH events) out of 2170 days (all the days in July–August from 1979 to 2013) and a composite analysis is performed on the selected events. To remain consistent with the observational analysis, the 26 onset days are selected regardless of sequence, and the 10 days before to 10 days after each selected onset day represent the corresponding duration for each EH event. For example, if 15 July and 18 August are selected as two random onset days, then 5–25 July and 8–28 August would be selected as two EH events. Second, the 2.5th and 97.5th percentiles of the 1000 simulations for each grid are chosen as the lower and upper thresholds of the 95% confidence level, respectively. Third, the number of significant grids in the composite field is counted for each simulation, and then the 1000 numbers are sorted as an increasing series N_{1000}. Finally, for each composite field of the 26 EH events from the observations, the number of significant grids N according to the Student's *t* test is counted and the percentage of N in the N_{1000} series is used as the confidence level of the observational composite field. (The field confidence level is marked above each panel in Figs. 4–9.)

To investigate the roles of ISOs in the occurrence of long-lived EH events over south China, the 5–25- and 30–90-day-filtered components are extracted from the original anomalies. Lanczos temporal filtering is employed to extract the corresponding ISO series. In section 5, during the analysis of the influence of ENSO on the interannual variation of EH frequency in south China, composite analysis and significance testing by the Student's *t* test with a confidence level of 90% are performed.

3. Temporal and spatial evolution of temperature anomalies associated with long-lived EH events in south China

Figure 1a shows the occurrence frequency of EH events with different durations. A large proportion of EH events last for no more than 3 days, accounting for 63% of all events (60/96). Therefore, the composite analyses of all EH events as presented by Chen et al. (2016) mainly describe the short-lived EH events. There are also some EH events that persist for a long period, with three events lasting for more than one month and the longest event lasting for 39 days (from 4 July to 11 August 2003). In total, the long-lived EH events (duration >5 days) account for 27% (26 events) of all EH events, comprising 63% (274 days) of all EH days.

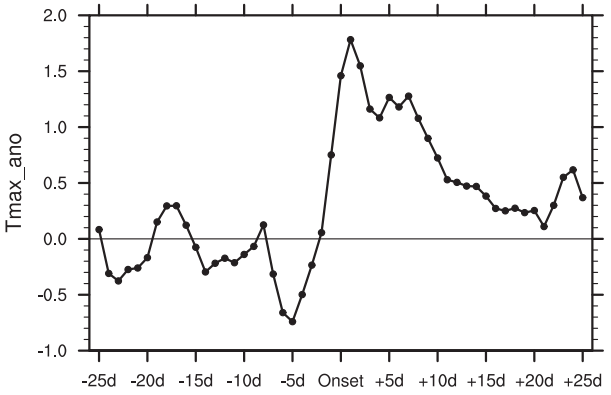

FIG. 2. Composite evolution of daily T_{max} anomalies (°C) from 25 days before to 25 days after the onset days of long-lived EH events. The temperature is averaged over the observational stations in south China.

The composite evolution of the temperature anomalies averaged over south China around the onset days of long-lived EH events is displayed in Fig. 2. The temperature anomalies show small oscillations before the EH onset days, with negative anomalies from −7 to −3 days. Then, the temperature obviously increases beginning on day −1, reaches the warmest on day +1 with an amplitude of +1.8°C, and then remains above +1.0°C (+0.5°C) until day +8 (day +10). Afterward, the temperature gradually decreases but stays abnormally positive. Overall, the warmer air conditions could last for approximately 10 days during long-lived EH events, apparently longer than the short-lived EH events, which last for less than 5 days (shown in Fig. 3c).

Figure 3 compares the evolution of the original temperature anomalies with the corresponding 5–25- and 30–90-day-filtered components around the long-lived EH onset days and end days, and the evolution around short-lived EH onset days are also shown for comparison. For the onset of long-lived EH events, the 5–25-day-filtered component adequately captures the original oscillations before the onset day and the reversal from a negative anomaly to a positive anomaly from −2 to −1 day (Fig. 3a). The 5–25-day-filtered component plays a predominant role in the original warming before +3 days. The warming associated with

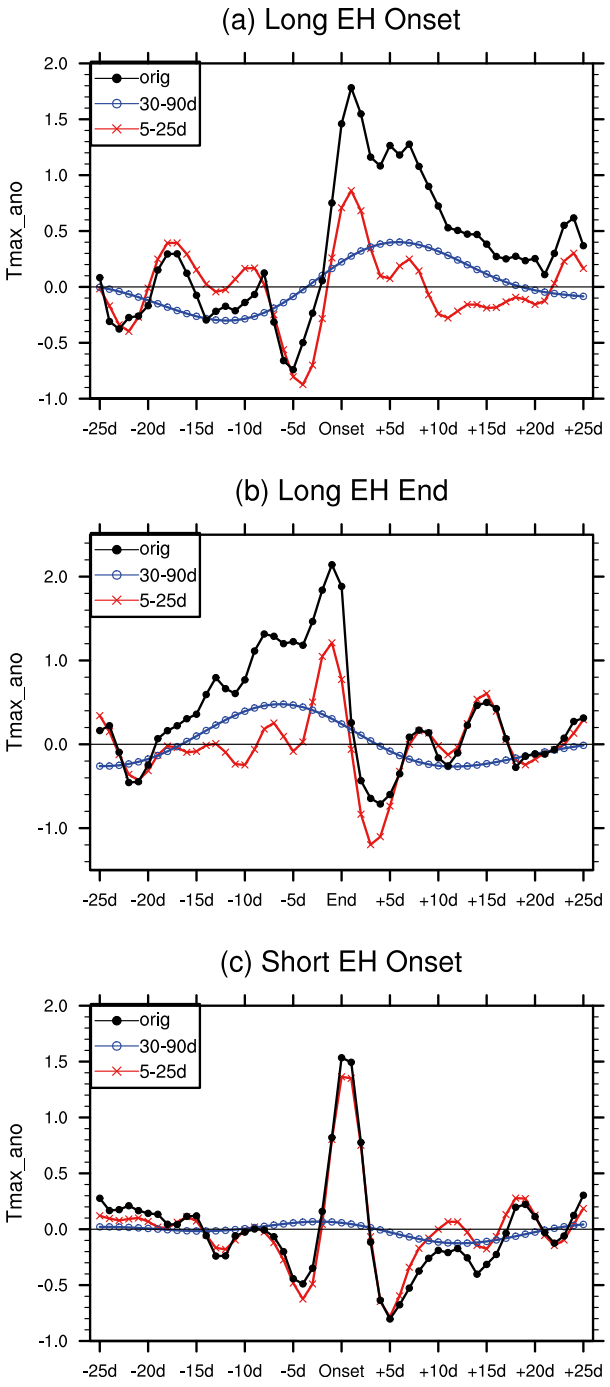

FIG. 3. Composite evolution of the daily T_{max} anomalies (°C) averaged over the observational stations in south China (black lines) and the corresponding 5–25- (red lines) and 30–90-day-filtered (blue lines) components from 25 days before to 25 days after the (a) onset days of long-lived EH events, (b) end days of long-lived EH events, and (c) onset days of short-lived EH events.

the 5–25-day oscillation reaches the maximum at +1 day (+0.9°C) and accounts for 48% of the original warming on the onset day and +1 day. In contrast, the 30–90-day-filtered component is in a positive phase beginning on the onset day and contributes to the original warming after onset. The warming contributed by the 30–90-day oscillation gradually increases after EH onset, with a peak amplitude of +0.4°C at +6 days and the largest ratio of 53% at +11 days. The warming associated with the 30–90-day oscillation becomes dominant, while the 5–25-day oscillation becomes weak after +3 days. Therefore, it is suggested that the 5–25-day oscillation is vital to triggering the EH, while the 30–90-day oscillation is important for the persistence of higher temperature during long-lived EH events.

The composite temperature evolutions around the end days of long-lived EH events are symmetric to those around the onset days (Fig. 3b). On the one hand, the 30–90-day-filtered component is in its positive phase before the end day and the positive phase plays an important role in the persistent warming before −3 days. On the other hand, the 5–25-day-filtered component adequately captures the original anomaly beginning on −3 days, playing a predominant role in the warming during the late stage of the EH events and the termination of long-lived EH. Compared to long-lived EH events, the temperature evolutions for short-lived EH events are essentially different. The 5–25-day-filtered component accounts for the majority of the original temperature anomaly during the whole process, while the 30–90-day oscillation is negligible (Fig. 3c). Therefore, it is implied that ISO activities associated with long-lived EH events and short-lived EH events are different.

Figures 4 and 5 demonstrate the composite spatial evolutions of temperature anomalies around the onset day and end day of long-lived EH events, including the original anomaly, 5–25- and 30–90-day-filtered anomalies. Hereafter, the anomalies on the onset and end days, and the adjacent nonoverlapping 3-day means are analyzed to exclude synoptic variations. For the original anomaly, anomalous cooling occurs over south China from −6 to −4 days before the onset day and then quickly diminishes and turns into significant warming on the onset day with an amplitude of over +2°C (Figs. 4a–c). Afterward, the warming over south China remains and is still significant from +4 to +6 days (Figs. 4d–e). The composite anomaly of the 5–25-day-filtered component resembles the original anomaly in the early stage from −6 to +3 days, with a negative anomaly over south China from −6 to −4 days that turns into a positive anomaly beginning on the onset day until +3 days (Figs. 4f–i). The warming associated with the 5–25-day

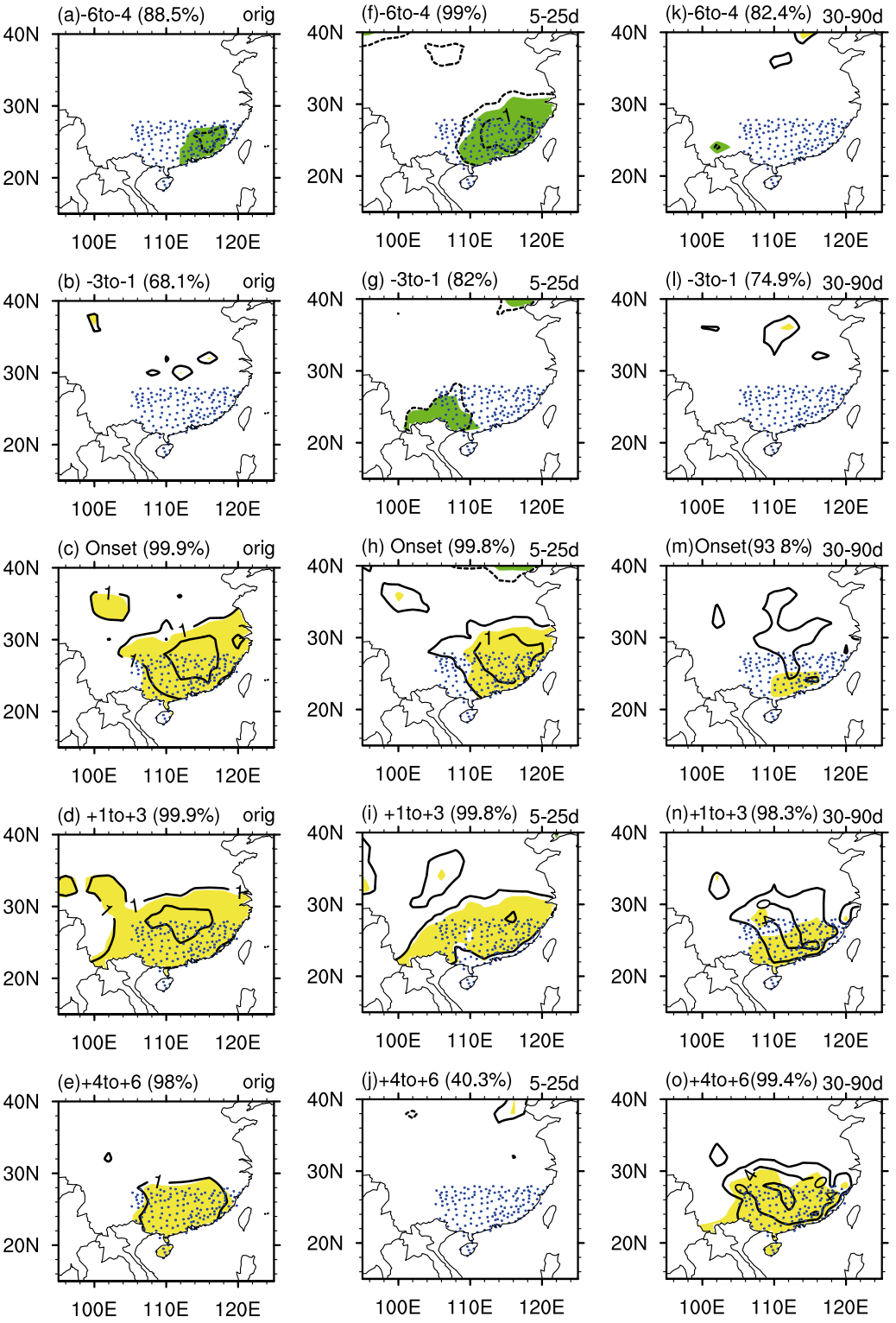

FIG. 4. Composite spatial evolutions of the nonoverlapping 3-day mean T_{max} anomalies around the onset days of long-lived EH events (°C): (a)–(e) The original anomaly (contour interval of 1°C), (f)–(j) the 5–25-day-filtered component (contour interval of 0.5°C), and (k)–(o) the 30–90-day-filtered component (contour interval of 0.1°C). The solid contours (yellow shading) denote positive anomalies, and the dashed contours (green shading) denote negative anomalies. The shaded areas are statistically significant at the 95% confidence level. The blue dots indicate the stations in south China. The percentages in the parentheses above the panels denote the confidence levels of the field significance testing, and the same is true in the following figures.

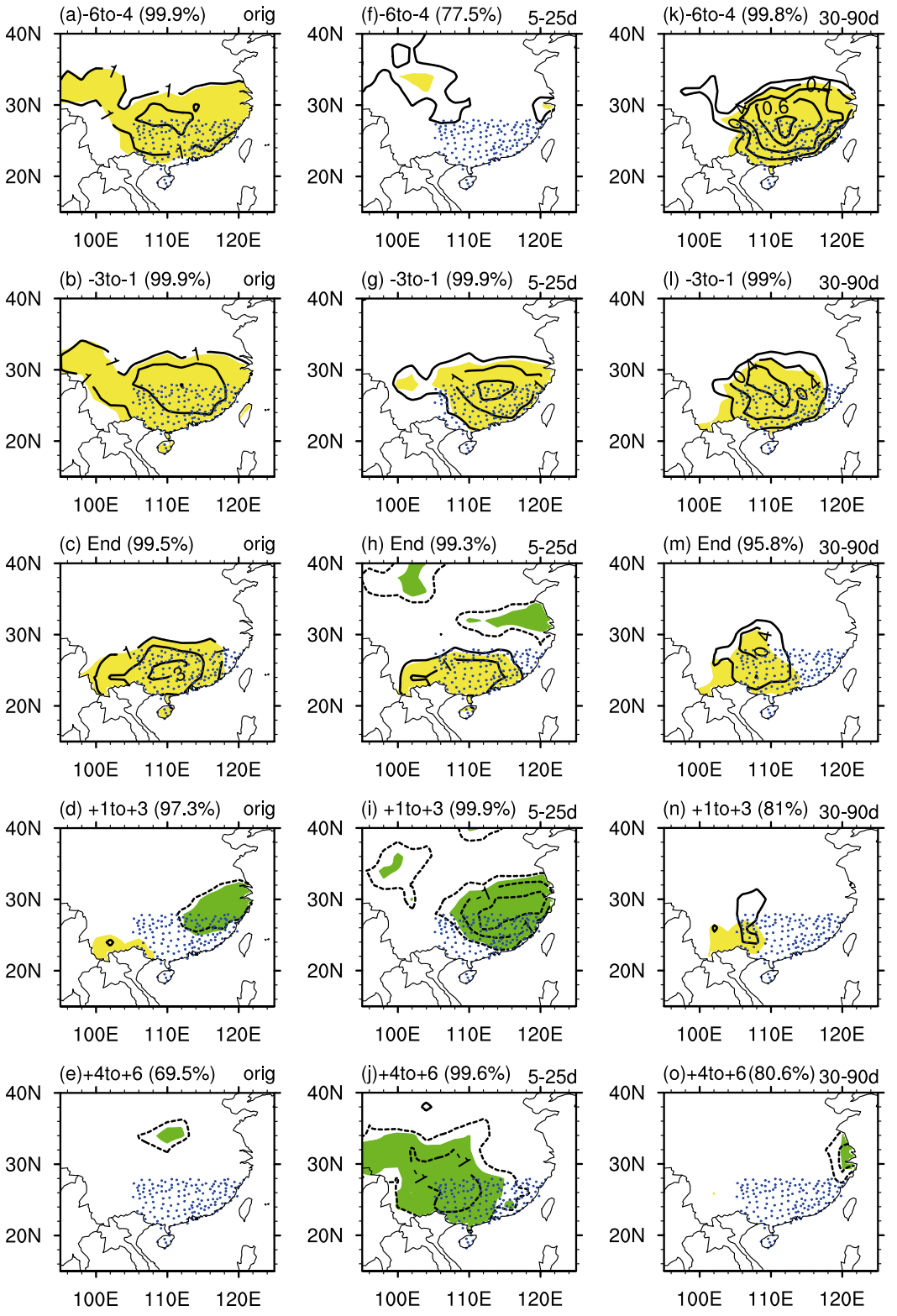

FIG. 5. As in Fig. 4, but for the anomalies around the end days of long-lived EH events.

oscillation reaches +1°C over south China on the onset day, accounting for approximately half of the original warming (Fig. 4h). In contrast, the 30–90-day-filtered component shows a weak anomaly before the onset day and then a significant positive anomaly develops over south China after the onset day (Figs. 4k–o). The warming associated with the 30–90-day oscillation becomes important during the late stage after onset, and the warming amplitude over south China reaches +0.5°C between +4 and +6 days, accounting for approximately half of the original warming (Fig. 4o).

The spatial evolution of the temperature anomalies around the EH end day display characteristics symmetrical to those around the onset day (Fig. 5). For the original anomaly, the warming over south China is quite strong beginning on −6 days to the end day and then is gradually replaced by anomalous cooling afterward (Figs. 5a–e). The early persistent warming before the end day is related to the 30–90-day oscillation (Fig. 5k), while the reversal from warming to cooling from −3 to +3 days is mostly due to the 5–25-day oscillation (Figs. 5g–i). Thereby, it can be inferred that the 5–25-day oscillation is responsible for the transformation of the temperature anomaly leading to the onset and termination of EH events, that is, from a negative anomaly to a positive anomaly or vice versa, while the 30–90-day oscillation favors the continuous warming during long-lived EH events.

4. Evolution of circulation anomalies and ISOs associated with long-lived EH events in south China

The lower-tropospheric circulation anomalies are analyzed in this section to detect the causes of the temperature anomalies during long-lived EH events. In fact, an empirical orthogonal function (EOF) analysis of the 500-hPa geopotential height anomalies on EH days over the Eurasian continent has also been performed, but no principal component was found to be significantly related to the length or strength of EH events (not shown). Therefore, only the analysis results of the lower-tropospheric circulation are presented. Figure 6 shows the evolution of the 700-hPa wind anomalies around the EH onset day. For the original anomaly, there is a significant anticyclone over the western Pacific and a discernible cyclone over south China from −6 to −4 days before the onset day (Fig. 6a). Then, the anomalous cyclone vanishes while the anomalous anticyclone strengthens and propagates northwestward, and south China is dominated by the anticyclonic anomaly on the onset day (Figs. 6b,c). The dominance of an anomalous anticyclone results in anomalous subsidence, lower humidity, and subsequently more solar radiation at the surface, favoring the occurrence of higher temperatures (not shown). After the onset day, the anticyclone remains over south China albeit getting weaker, and the anomalous anticyclone is still significant from +4 to +6 days (Figs. 6d,e). The prolonged dominance of an anticyclonic anomaly favors the maintenance of higher temperatures over south China.

The 5–25-day-filtered circulation anomaly resembles the original anomaly from −6 days to the onset day (Figs. 6f–h). There is an anomalous anticyclone–cyclone pair over the western Pacific and south China from −6 to −4 days, and the cyclone over south China appears to be significant (Fig. 6f). The pair propagates northwestward and the anticyclonic anomaly strengthens and governs south China on the onset day (Figs. 6g,h). The amplitude of the 5–25-day-filtered anomaly accounts for approximately two-thirds of the original anomaly, indicating the importance of the 5–25-day oscillation in the triggering of an EH event by the circulation anomalies, which propagates from the western Pacific.

The 30–90-day-filtered circulation demonstrates a persistent anticyclonic anomaly from −6 to +6 days, which gradually strengthens and propagates from the western Pacific to south China (Figs. 6k–o). The anomalous anticyclone is quite weak at the beginning but becomes obvious beginning on the onset day (Figs. 6k–m). After the onset day, the anticyclonic anomaly remains over south China, which resembles the original anomaly and accounts for approximately one-third of the amplitude (Figs. 6n,o). Therefore, the anticyclonic component of the 30–90-day oscillation, propagating from the western Pacific, contributes to the persistence of the original anticyclonic anomaly and higher temperatures over south China after the onset of an EH event.

The circulation anomalies around the end day of long-lived EH events are somewhat symmetrical to those around the onset day (Fig. 7). For the original anomaly, there is a significant anticyclone over south China before the end day, accompanied by a cyclone to the southeast (Figs. 7a,b). The anticyclone–cyclone pair propagates northwestward as the cyclonic (anticyclonic) component gets stronger (weaker). The cyclonic component is centered over the eastern edge of south China on the end day and moves to south China from +1 to +3 days (Figs. 7c,d). The approach of the cyclonic anomaly favors lower temperatures and leads to the termination of EH events.

The 5–25-day-filtered anomaly shows an anticyclone to the southeast of south China from −6 to −4 days, and the anticyclone moves to south China with a cyclone developing over the western Pacific between −3

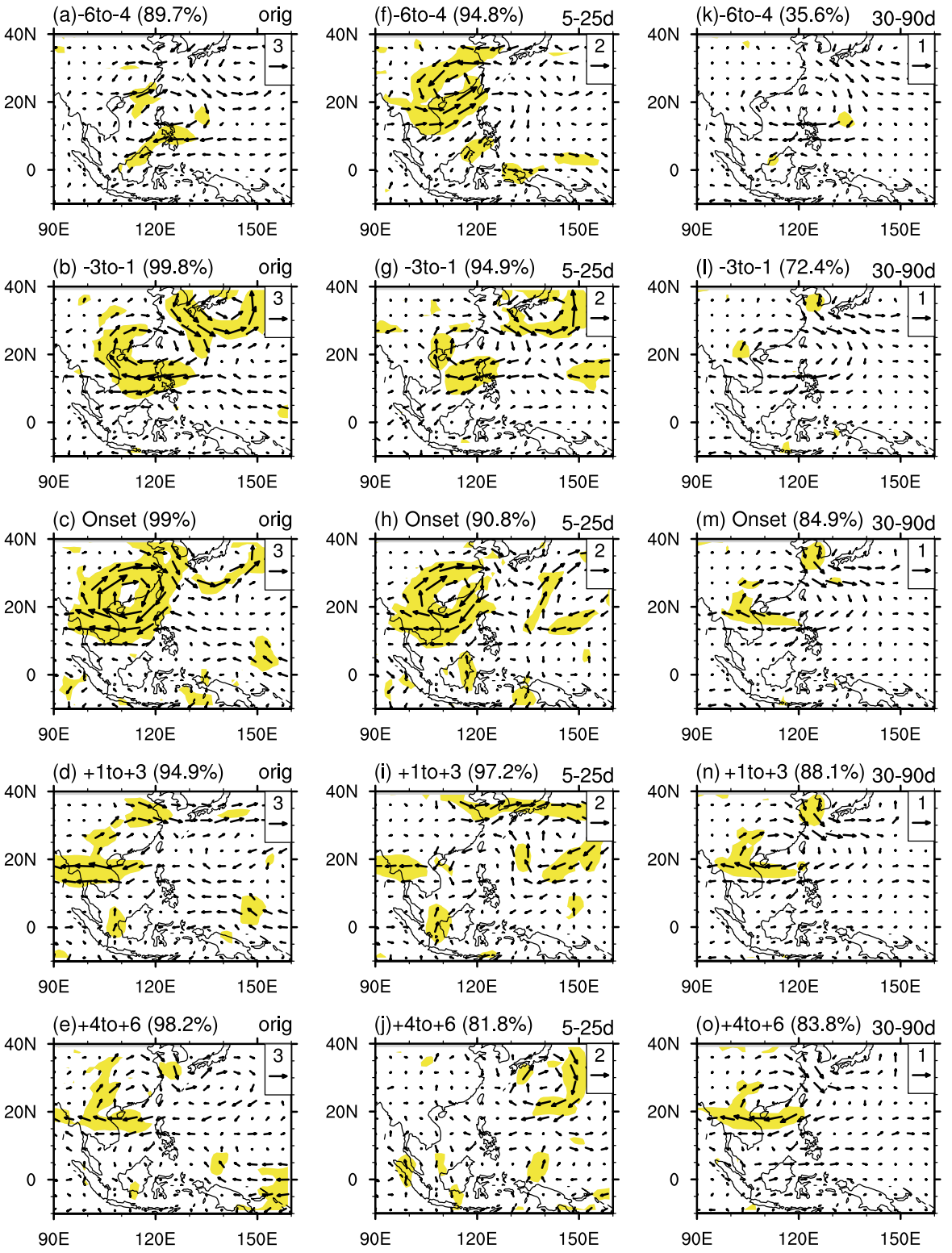

FIG. 6. As in Fig. 4, but for the 700-hPa wind anomalies (vectors; m s^{-1}). The shaded areas indicate that either the zonal or meridional wind anomaly is significant at the 95% confidence level.

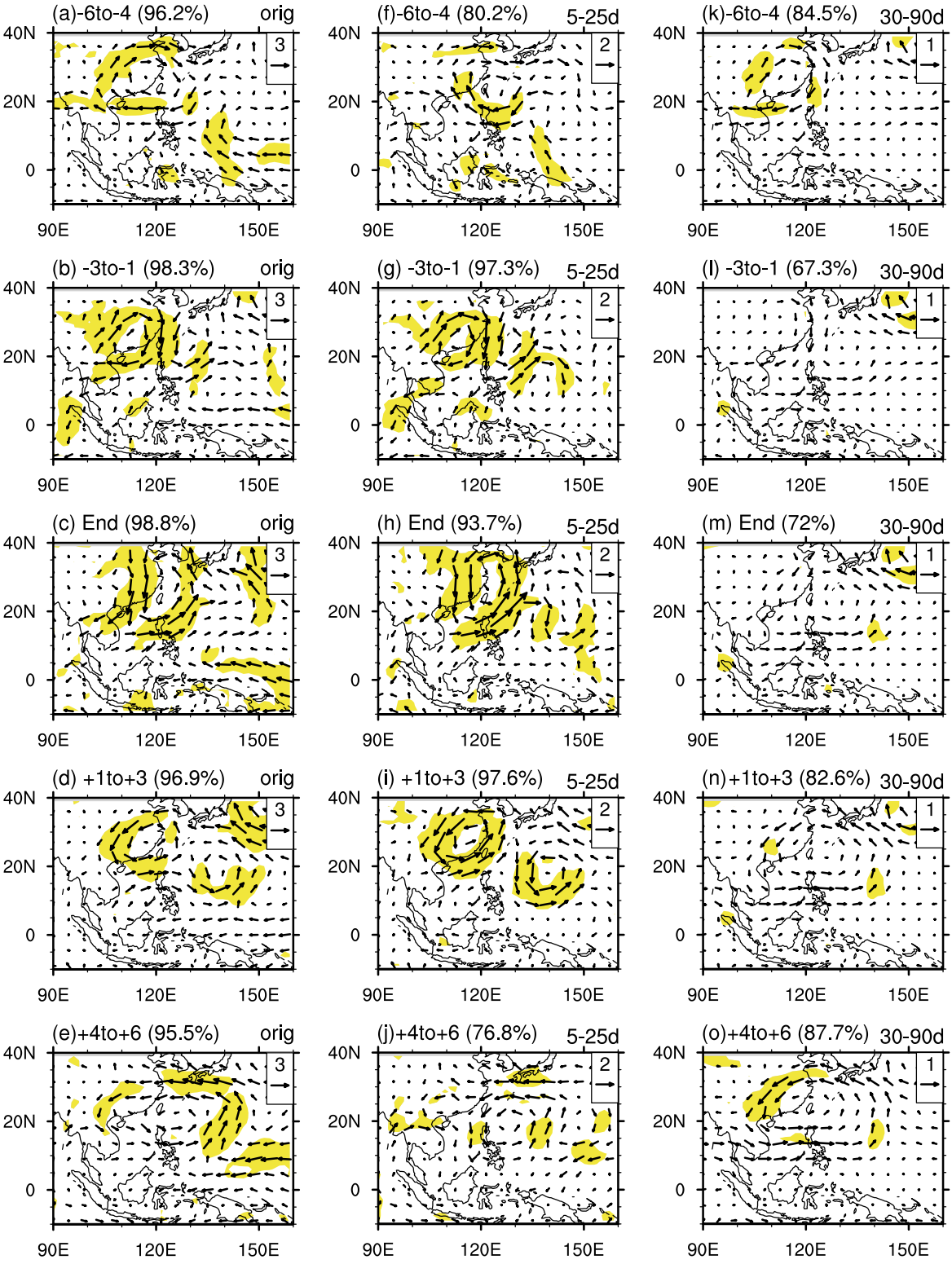

FIG. 7. As in Fig. 6, but for the anomalies around the end days of long-lived EH events.

and −1 day, and then the cyclone moves northwestward to south China (Figs. 7f–i). The 5–25-day-filtered anomaly is similar to the original anomaly from −3 to +3 days, accounting for approximately two-thirds of the original amplitude and contributing greatly to the termination of long-lived EH events. In contrast, the 30–90-day-filtered anomaly presents a significant anticyclone over south China from −6 to −4 days, and then the anticyclone gradually weakens and turns into a cyclonic anomaly after the end day (Figs. 7k–o). The anticyclone from −6 to −4 days is similar to the original anomaly and favors the persistent warming over south China before the end day. Therefore, the cyclonic component associated with the 5–25-day oscillation is vital for the termination of EH events, while the persistent anticyclonic component associated with the 30–90-day oscillation is favorable for the maintenance of warming during EH events.

Furthermore, the OLR is analyzed to detect the heat source of the ISO activities that influence south China. Figure 8 displays the evolutions of OLR anomalies around the onset day of long-lived EH events. The original OLR anomaly shows a wave train originating from the Maritime Continent over the tropical western Pacific and propagating northwestward to south China (Figs. 8a–e). From −6 to −4 days, there is one positive OLR anomaly centered to the east of the Philippines and two negative centers located over the tropical Maritime Continent and south China (Fig. 8a). Then, the positive anomaly migrates northwestward and is located over south China on the onset day (Figs. 8b,c). The positive OLR anomaly over south China indicates the inhibition of convection, favoring higher temperatures and resulting in the onset of EH. After the onset day, a positive OLR anomaly remains over south China and favors the maintenance of higher temperatures (Figs. 8d,e).

The 5–25-day-filtered OLR anomaly resembles the original anomaly from −6 to +3 days, showing a wave train originating from the tropical Maritime Continent and propagating northwestward to south China (Figs. 8f–i). South China is significantly dominated by the negative phase of the OLR anomaly from −6 to −4 days and by the positive phase on the onset day (Figs. 8f and 8h, respectively). The positive OLR anomaly associated with the 5–25-day oscillation accounts for approximately two-thirds of the original anomaly over south China on the onset day, which contributes greatly to triggering the EH events.

In contrast, the 30–90-day-filtered OLR shows a pair of positive–negative anomalies that gradually propagate northwestward from the tropical western Pacific to south China, and south China is continuously influenced by the positive phase of the OLR anomaly from −6 to +6 days (Figs. 8k–o). The 30–90-day-filtered anomalies show larger zonal regimes and slower migration compared with the 5–25-day-filtered anomalies. Before the onset day, the positive anomaly is centered to the east of the Philippines, and the negative anomaly is centered over the tropical Maritime Continent (Figs. 8k,l). Beginning on the onset day, the significant positive anomaly reaches south China and slowly shifts northwestward (Figs. 8m–o). South China is dominated by a significant positive OLR anomaly from +1 to +6 days for the 30–90-day-filtered component, accounting for approximately one-third of the original anomaly and favoring the persistence of higher temperatures.

Figure 9 demonstrates the evolution of OLR anomalies around the long-lived EH end day. For the original anomaly, there is a pair of positive–negative anomalies propagating from the western Pacific to south China, along a near-westward path at approximately 20°N (Figs. 9a–e). A positive anomaly occurs over south China before the end day and is replaced by the negative anomaly from the western Pacific beginning on the end day. The approach of the negative OLR anomaly leads to lower temperatures and terminates the EH events. Both the 5–25- and 30–90-day-filtered anomalies over south China show transitions from a positive phase to a negative phase around the EH end day, but the former transition occurs at the end day and the latter occurs from +4 to +6 days (Figs. 9h and 9o, respectively). When comparing the original anomaly with the 5–25- and 30–90-day-filtered anomalies, the original positive OLR anomaly during the early days from −6 to −4 days is consistent with the positive phase of the 30–90-day oscillation (Figs. 9a,k), while the transformation from a positive to a negative anomaly from −3 to +3 days is intimately related to the phase transition of the 5–25-day oscillation (Figs. 9b–d,g–i).

Figures 10 show the propagations of the OLR anomalies along the northwestward (westward) path from the western Pacific to south China during a longer time segment from −33 to +33 days around the onset day (end day) to better illustrate the origins of the oscillations. The northwestward path is along the positive–negative OLR anomaly centers around the EH onset day, denoted by the dashed line from 5°S, 140°E to 30°N, 105°E, as shown in Fig. 8b. The original and 5–25- and 30–90-day-filtered anomalies around the onset day clearly propagate northwestward from the tropical western Pacific to south China, and the initial anomalies could be derived from the near-equatorial region (Figs. 10a–c). For the area of south China around 21°N, 114°E, the evolution of the original anomaly from negative to positive between −18 and +18 days is

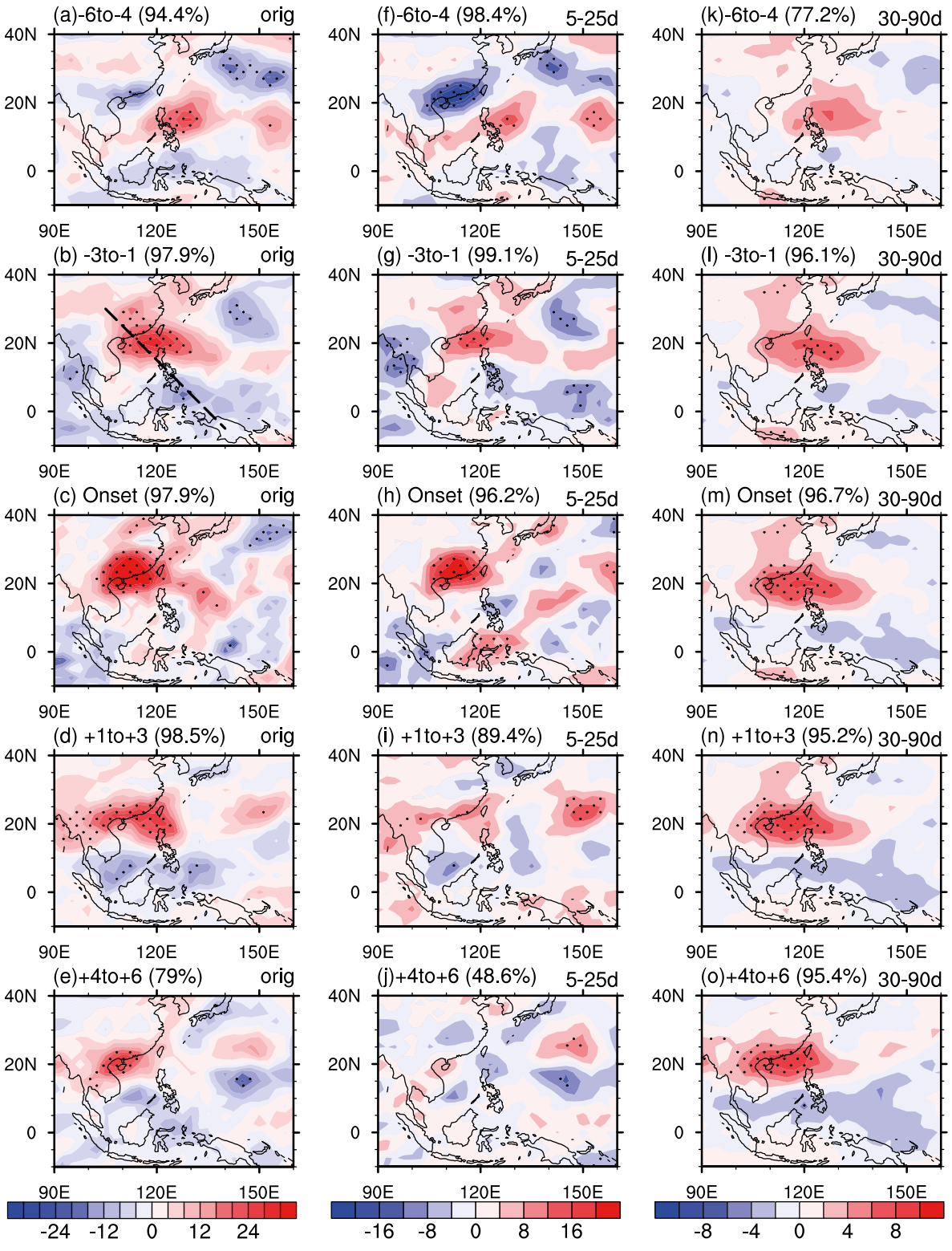

FIG. 8. As in Fig. 4, but for the OLR anomalies (shading; W m^{-2}). The shaded intervals are 4 W m^{-2} for the original anomalies and 5–25-day-filtered anomalies and 2 W m^{-2} for the 30–90-day-filtered anomalies. The dotted areas are significant at the 95% confidence level. [The dashed line in (b) lying along the anomaly centers from 5°S, 140°E to 30°N, 105°E denotes the path used in Figs. 10a–c to depict the northwestward propagation of the convective activities.]

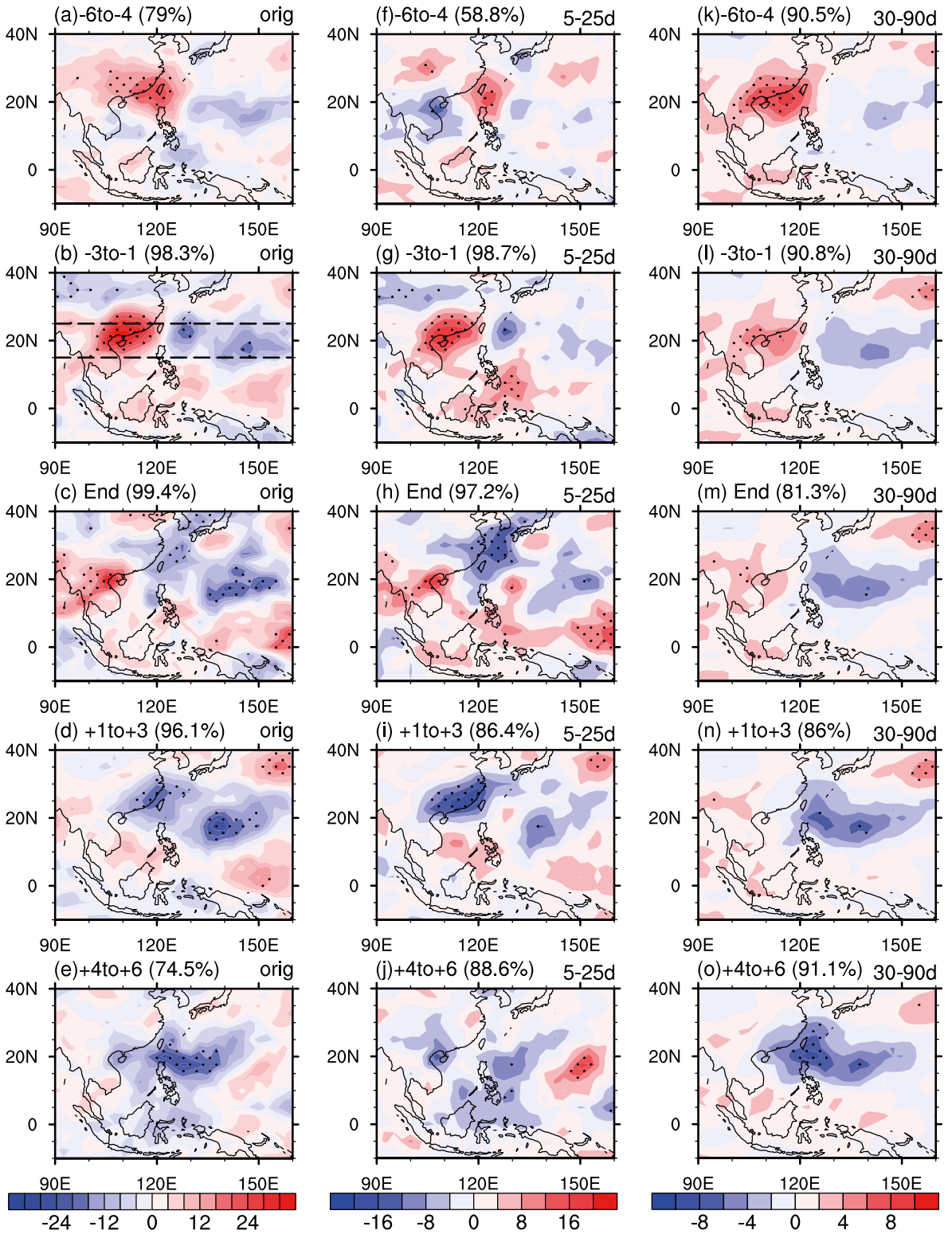

FIG. 9. As in Fig. 8, but for the OLR anomalies around the end days of long-lived EH events. The two dashed lines lying along 15° and 25°N in (b) denote the meridional range over which the anomalies are averaged to illustrate the westward propagation of convective activities (later presented in Figs. 10d–f).

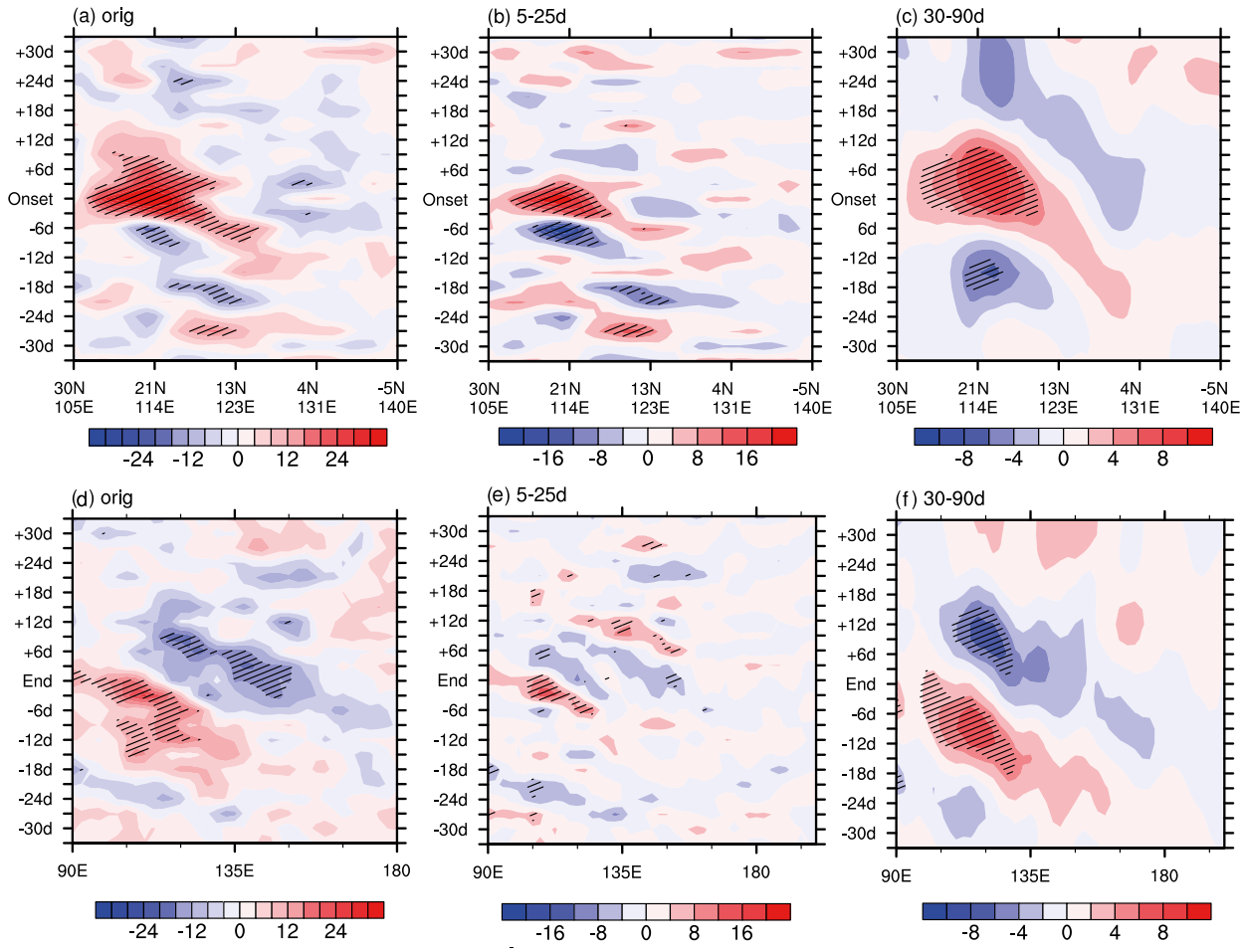

FIG. 10. The northwestward propagation of the (a) original and (b) 5–25- and (c) 30–90-day-filtered OLR anomalies around the onset days of long-lived EH events. The northwestward path lies from 5°S, 140°E to 30°N, 105°E, as denoted by the dashed line in Fig. 8b. The westward propagation of the (d) original and (e) 5–25- and (f) 30–90-day-filtered OLR anomalies around the end days. The westward path is the meridional mean between 15° and 25°N, denoted by the two dashed lines in Fig. 9b. The units and shaded intervals are the same as in Fig. 8. The areas marked by hatching are significant at the 95% confidence level.

accompanied by the phase transitions of both the 5–25- and 30–90-day oscillations. The phase transition cycle of the 5–25-day oscillation from −9 to +3 days resembles the original anomaly and favors the onset of EH events, while the positive phase of the 30–90-day oscillation contributes greatly to the original anomaly from +3 to +12 days.

Compared to the northwestward propagation of the OLR anomaly around the onset day, the anomaly around the end day appears to propagate westward (Fig. 9). Hence, the path that is analyzed for the end day is chosen as the meridional mean between 15° and 25°N, denoted by the dashed lines in Fig. 9b. The anomalies propagate from the western Pacific to south China for the original and 5–25- and 30–90-day-filtered anomalies (Figs. 10d–f). For the area of south China located between 105° and 120°E, the transition of the original OLR anomaly from positive to negative around the end day is associated with the phase transitions of both the 5–25- and 30–90-day oscillations. The original OLR anomaly over south China is presented as a persistent positive anomaly from −18 days to the end day and is then replaced by the negative anomaly originating from the east (Fig. 10d). The original persistent positive anomaly before −3 days is closely related to the positive phase of the 30–90-day oscillation (Fig. 10f), while the reversal of the original anomaly from −3 to +3 days is mainly associated with the 5–25-day oscillation (Fig. 10e). Thereby, it is demonstrated that the ISOs originate from the tropical western Pacific and propagate northwestward to south China, and different ISO modes play important roles at different stages of the long-lived EH events.

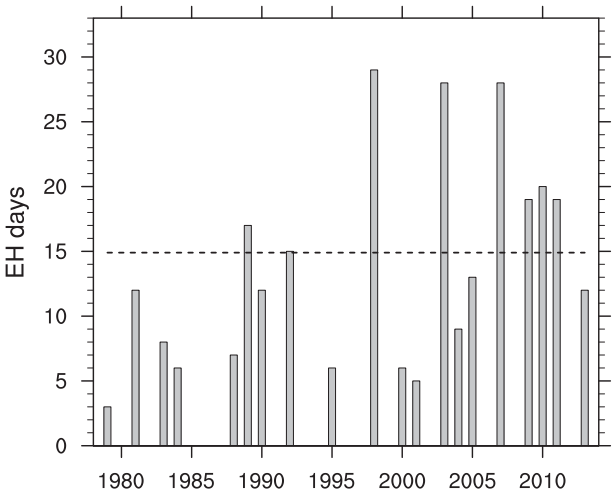

FIG. 11. Annual frequency (days) of long-lived EH days in south China. The threshold for selecting the years with high EH frequencies, that is, 15 days yr^{-1}, is denoted by the dashed line. The years without an EH day are selected as years with low EH frequencies.

5. Influence of ENSO on the annual frequency of long-lived EH days in south China

This section further detects the influence of tropical SSTAs on the annual frequency of long-lived EH days in south China. Figure 11 shows the annual frequency of long-lived EH days from 1979 to 2013, and the frequency presents an obvious interannual variation. To investigate the causes of the interannual variation of the EH frequency, we select the years with high EH frequencies and low EH frequencies to perform the composite analysis. The high-frequency years are defined as the years with more than 15 EH days (standard deviation greater than 0.7), and the low-frequency years are defined as the years without an EH day (standard deviation less than −0.7). In total, there are 8 (15) years with high (low) EH frequencies, which are listed in Table 1. In the following, only the composite differences between the high index years and the low index years are presented. We also evaluated the composite anomalies for high index years and low index years, and the former (latter) are similar to (opposite from) the composite differences but with a lower confidence level (not shown).

Figure 12 demonstrates the composite differences of SSTAs between the years with high and low EH frequencies, including the SSTAs in the preceding winter, the simultaneous summer, and the incoming winter. Significant warming occurs over the eastern Pacific in the preceding winter and evolves into significant cooling over the central–eastern Pacific during the simultaneous summer and incoming winter (Figs. 12a–c). The higher frequency of EH in south China is associated with the decaying phase of El Niño during the preceding winter and the developing phase of La Niña during the simultaneous summer, appearing as the transition phase from El Niño to La Niña.

To explore how ENSO influences the EH in south China, the Niño-3 index in the preceding winter is employed, and a composite analysis of the atmospheric circulation is performed according to the index. The Niño-3 index is computed as the SSTA averaged over 5°S–5°N, 150°–90°W during the preceding winter, denoted by the black box in Fig. 12a. The years with a Niño-3 index higher (lower) than 0.7 (−0.7) standard deviation are defined as El Niño (La Niña) years, and there are seven El Niño years and seven La Niña years, as listed in Table 1. Figure 13a shows the composite difference of the lower-tropospheric wind anomalies during the summer between El Niño and La Niña years. There is a significant anticyclonic anomaly over south China, which likely emerges during the summer following El Niño. The anticyclonic anomaly favors higher temperatures over south China. Similarly, the composite difference of the lower-tropospheric wind between the years with high and low frequencies of EH also presents an anomalous anticyclone over south China (Fig. 13b). This similarity implies that El Niño (La Niña) in the preceding winter could enhance (reduce) the occurrence frequency of EH in south China through favoring an anomalous anticyclone (cyclone) over south China during the following summer.

The present results tend to be consistent with Wang et al. (2014). However, caution should be used when comparing the present study with their results because of some crucial differences between these studies. First, the locations are different: this study focuses on south China, while the other study focuses on the lower reach of the Yangtze River basin. Second, this study distinguishes the long-lived EH events from the short-lived EH events, but the other study merges the events. In actuality, there are substantial differences between Fig. 11 in this study and Fig. 2c in Wang et al. (2014), which show the annual frequency of long-lived EH days and the time coefficient of the first EOF mode of all EH days, respectively. Furthermore, we examined the SSTAs associated with the interannual variation of short-lived EH days in south China based on a composite analysis, the same as Fig. 12. The SSTA pattern associated with short-lived EH is opposite from that associated with long-lived EH to some extent, but the significance is lower (not shown). Therefore, it is specified in the present study that the correspondence between more (less) EH days in the summer and El Niño

TABLE 1. List of years with high and low EH frequencies and high and low Niño-3 indices in the preceding winter.

Index	No. of yr	Years
High EH frequency (frequency ≥ 15 days; std dev > 0.7)	8	1989, 1992, 1998, 2003, 2007, 2009, 2010, and 2011
Low EH frequency (frequency = 0 days; std dev < −0.7)	15	1980, 1982, 1985, 1986, 1987, 1991, 1993, 1994, 1996, 1997, 1999, 2002, 2006, 2008, and 2012
High Niño-3 index (std dev > 0.7)	7	1983, 1987, 1992, 1995, 1998, 2003, and 2010
Low Niño-3 index (std dev < −0.7)	7	1985, 1989, 1999, 2000, 2006, 2008, and 2011

(La Niña) in the preceding winter is significant for long-lived EH but not for short-lived EH.

6. Conclusions

The large-scale circulation anomalies responsible for the occurrence of long-lived EH events in south China are investigated in the current study. The role of boreal summer ISO over the western Pacific is another focus, including the two profound ISO modes, namely, the 5–25-day oscillation and the 30–90-day oscillation. Accordingly, the 5–25- and 30–90-day-filtered data are extracted, together with the original anomalies, to analyze the causes of long-lived EH events in south China. Furthermore, the influence of ENSO on the annual frequency of long-lived EH days in south China is explored.

The temporal and spatial evolution of the temperature anomalies associated with long-lived EH events are first analyzed. The results show that the temperature over south China obviously increases around the EH onset day and then remains anomalously high for approximately 10 days on average and decreases around the EH end day. Both the 5–25- and 30–90-day oscillations contribute to the evolution of long-lived EH events in south China, but their relative roles vary at different stages of the EH events. The 5–25-day-filtered component shows obvious oscillations around the onset and end days of the EH events and adequately captures the rapid temperature increase or decrease, accounting for approximately half of the temperature variation. In contrast, the warming phase of the 30–90-day component gradually develops after the EH onset day. The warming associated with the 30–90-day oscillation peaks at +6 days and then the warming decays gradually. Hence, it can be concluded that the 5–25-day oscillation plays a vital role in triggering and terminating the EH events, and the 30–90-day oscillation is important for the persistence of higher temperatures during long-lived EH events.

The circulation anomalies associated with long-lived EH events are demonstrated as an anticyclone–cyclone pair that propagates northwestward from the western Pacific to south China before the EH onset day. The anticyclonic component migrates to south China on the onset day and then remains over south China after the onset. The anticyclonic anomaly is coupled with convection inhibition over south China, which increases the air temperature and favors the onset and persistence of EH events. A new cyclonic anomaly is generated over the western Pacific and moves westward to south China around the EH end day. The approach of a cyclonic anomaly and its dominance over south China is accompanied by abnormal active convection, terminating the higher temperatures and ending the EH events.

These circulation anomalies are intimately related to the ISOs of the tropical atmosphere. Both the 5–25- and 30–90-day-filtered OLR anomalies display an oscillating pattern over the western Pacific and south China that originates from the tropical Maritime Continent and propagates northwestward. The inactive convection

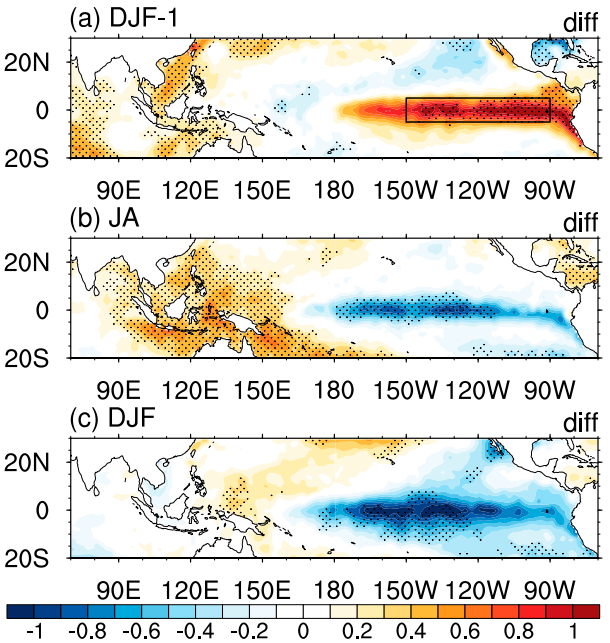

FIG. 12. Composite difference of SSTAs between the years with high EH frequencies and low EH frequencies. The SSTAs (°C) are averaged during the (a) preceding winter (DJF−1), (b) simultaneous summer [July–August (JA)], and (c) following winter (DJF). The dotted areas are significant at the 90% confidence level. The years used for composite analysis are listed in Table 1.

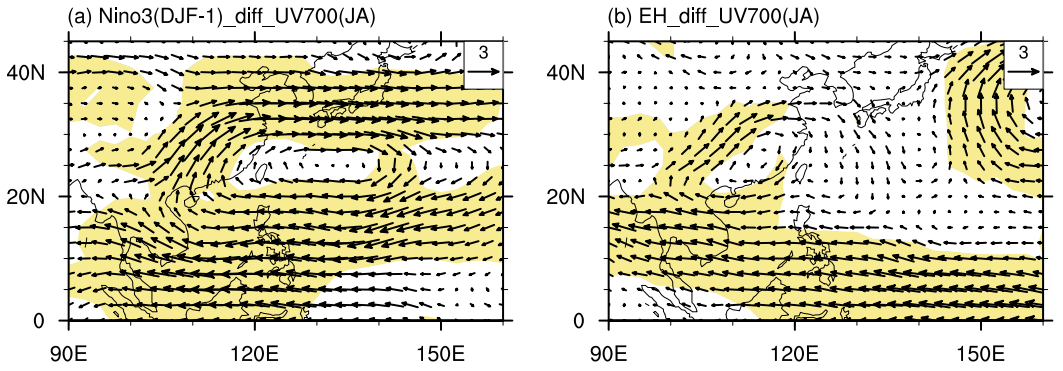

FIG. 13. Composite difference of the 700-hPa wind anomalies (vectors; m s^{-1}) (a) between El Niño and La Niña years and (b) between years with high EH frequencies and low EH frequencies. The shaded areas indicate that either the zonal or meridional wind anomaly is significant at the 90% confidence level. The years used for composite analysis are listed in Table 1.

phase of the 5–25-day oscillation migrates from the tropical western Pacific to south China around the onset day, leading to the initiation of EH. Afterward, the inactive convection associated with the 30–90-day oscillation develops over south China and becomes predominant, favoring the continuation of warming. Later, before the EH end day, the inactive convection of the 30–90-day oscillation decays, while the 5–25-day oscillation becomes dominant again, with active convection shifting from the western Pacific to south China and terminating the EH. Overall, the 5–25-day-filtered component accounts for approximately two-thirds of the original anomalies adjacent to the onset day and end day, and the 30–90-day-filtered component accounts for approximately one-third of the anomalies during the EH events. It is thus indicated that the synergy between the 5–25- and 30–90-day oscillations of the tropical atmosphere greatly contributes to the occurrence of long-lived EH events in south China.

Preliminary work has been conducted comparing various filters (e.g., 30–60 days) to the Madden–Julian oscillation (MJO) cycle based on the real-time multivariate MJO (RMM) index released by the Australian Bureau of Meteorology. The results show that long-lived EH days tend to occur more frequently during phases 1, 2, 5, and 6 of the MJO cycle, while they occur less frequently during phases 3, 4, 7, and 8 (not shown). However, the ratios of EH days to all days of each phase are not significantly distinguished (not shown). Accordingly, a question arises: why does the MJO exhibit such distinct days at different phases of the MJO? Further work should be undertaken to explore this question.

On the other hand, the annual frequency of long-lived EH days in south China is modulated by ENSO. Higher EH frequency is associated with the decaying phase of El Niño in the preceding winter and the developing phase of La Niña in the simultaneous summer. The warmer SST in the preceding winter over the eastern Pacific enhances the frequency of EH days by favoring an anomalous anticyclone over south China during the following summer.

The significant influences of ISO and ENSO on EH events indicate the possibility of medium-range and interannual forecasting of high temperatures in south China. More concretely, different ISO modes should be addressed when considering EH events with different lengths. For short-lived EH events, the 5–25-day oscillation is predominant during the entire process. In contrast, long-lived EH events result from the combined influences of the 5–25- and 30–90-day oscillations, with the 5–25-day oscillation important for triggering and terminating EH events and the 30–90-day oscillation contributing to persistent warming. At the same time, it is worth comparing the accuracy of the temperature forecast for long-lived and short-lived EH events in the current numerical weather forecasting systems, which would help improve the forecast accuracy. Furthermore, it is believed that the frequency of EH will generally increase under global warming. However, the regional trend of EH frequency is supposed to be affected by the changes in regional circulation patterns (Horton et al. 2015; Grotjahn et al. 2016). The present results suggest that special attention should be paid to the ISOs over the western Pacific and south China to better project the future changes of the EH events in south China.

Acknowledgments. We thank three reviewers for their comments and suggestions, which helped to improve the manuscript. This work is jointly supported by National Natural Science Foundation of China (Grants 41605027, 41320104007, and 41530530) and the National Key Research and Development Program (2016YFA0600601).

REFERENCES

Alexander, L. V., and Coauthors, 2006: Global observed changes in daily climate extremes of temperature and precipitation. *J. Geophys. Res.*, **111**, D05109, https://doi.org/10.1029/2005JD006290.

Black, E., M. Blackburn, G. Harrison, B. Hoskins, and J. Methven, 2004: Factors contributing to the summer 2003 European heatwave. *Weather*, **59**, 217–223, https://doi.org/10.1256/wea.74.04.

Chen, J., Z. Wen, R. Wu, Z. Chen, and P. Zhao, 2015: Influences of northward propagating 25–90-day and quasi-biweekly oscillations on eastern China summer rainfall. *Climate Dyn.*, **45**, 105–124, https://doi.org/10.1007/s00382-014-2334-y.

Chen, R., and R. Lu, 2014a: Large-scale circulation anomalies associated with 'tropical night' weather in Beijing, China. *Int. J. Climatol.*, **34**, 1980–1989, https://doi.org/10.1002/joc.3815.

——, and ——, 2014b: Dry tropical nights and wet extreme heat in Beijing: Atypical configurations between high temperature and humidity. *Mon. Wea. Rev.*, **142**, 1792–1802, https://doi.org/10.1175/MWR-D-13-00289.1.

——, and ——, 2015: Comparisons of the circulation anomalies associated with extreme heat in different regions of eastern China. *J. Climate*, **28**, 5830–5844, https://doi.org/10.1175/JCLI-D-14-00818.1.

——, Z. Wen, and R. Lu, 2016: Evolution of the circulation anomalies and the quasi-biweekly oscillations associated with extreme heat events in southern China. *J. Climate*, **29**, 6909–6921, https://doi.org/10.1175/JCLI-D-16-0160.1.

Chen, Y. and P. Zhai, 2017: Simultaneous modulations of precipitation and temperature extremes in Southern parts of China by the boreal summer intraseasonal oscillation. *Climate Dyn.*, **49**, 3363–3381 https://doi.org/10.1007/s00382-016-3518-4.

Collins, D. A., P. M. Della-Marta, N. Plummer, and B. C. Trewin, 2000: Trends in annual frequencies of extreme temperature events in Australia. *Aust. Meteor. Mag.*, **49**, 277–292.

Coumou, D., and S. Rahmstorf, 2012: A decade of weather extremes. *Nat. Climate Change*, **2**, 491–496, https://doi.org/10.1038/nclimate1452.

Dee, D. P., and Coauthors, 2011: The ERA-Interim reanalysis: Configuration and performance of the data assimilation system. *Quart. J. Roy. Meteor. Soc.*, **137**, 553–597, https://doi.org/10.1002/qj.828.

Fang, Y., and M. Jian, 2011: Diagnosis study of persistent heat waves in South China during summer 2003 (in Chinese). *J. Trop. Oceanogr.*, **30**, 30–37.

Gao, M., J. Yang, B. Wang, S. Zhou, D. Gong, and S.-J. Kim, 2017: How are heat waves over Yangtze River valley associated with atmospheric quasi-biweekly oscillation? *Climate Dyn.*, https://doi.org/10.1007/s00382-017-3526-z, in press.

Gao, R., L. Wang, and G. Gao, 2008: The trend of variation in high temperature days during 1956–2006 in China. *Adv. Climate Change Res.*, **4**, 177–181.

Gershunov, A., D. R. Cayan, and S. F. Iacobellis, 2009: The great 2006 heat wave over California and Nevada: Signal of an increasing trend. *J. Climate*, **22**, 6181–6203, https://doi.org/10.1175/2009JCLI2465.1.

Grotjahn, R., and Coauthors, 2016: North American extreme temperature events and related large scale meteorological patterns: A review of statistical methods, dynamics, modeling, and trends. *Climate Dyn.*, **46**, 1151–1184, https://doi.org/10.1007/s00382-015-2638-6.

Horton, D. E., N. C. Johnson, D. Singh, D. L. Swain, B. Rajaratnam, and N. S. Diffenbaugh, 2015: Contribution of changes in atmospheric circulation patterns to extreme temperature trends. *Nature*, **522**, 465–469, https://doi.org/10.1038/nature14550.

IPCC, 2013: Summary for policymakers. *Climate Change 2013: The Physical Science Basis*, T. F. Stocker et al., Eds., Cambridge University Press, 3–29.

Jia, X., and S. Yang, 2013: Impact of the quasi-biweekly oscillation over the western North Pacific on East Asian subtropical monsoon during early summer. *J. Geophys. Res. Atmos.*, **118**, 4421–4434, https://doi.org/10.1002/jgrd.50422.

Kilbourne, E. M., 1997: Heat waves and hot environments. *The Public Health Consequences of Disasters*, E. K. Noji, Ed., Oxford University Press, 245–269.

Kunkel, K. E., X.-Z. Liang, and J. H. Zhu, 2010: Regional climate model projections and uncertainties of U.S. summer heat waves. *J. Climate*, **23**, 4447–4458, https://doi.org/10.1175/2010JCLI3349.1.

Lau, N. C., and M. J. Nath, 2012: A model study of heat waves over North America: Meteorological aspects and projections for the twenty-first century. *J. Climate*, **25**, 4761–4784, https://doi.org/10.1175/JCLI-D-11-00575.1.

Lelieveld, J., Y. Proestos, P. Hadjinicolaou, M. Tanarhte, E. Tyrlis, and G. Zittis, 2016: Strongly increasing heat extremes in the Middle East and North Africa (MENA) in the 21st century. *Climatic Change*, **137**, 245–260, https://doi.org/10.1007/s10584-016-1665-6.

Li, T., Y. Du, Y. Mo, Z. Du, L. Huang, and Y. Cheng, 2014: Human risk assessment of heat wave based on vulnerability: A review of recent studies. *J. Environ. Health*, **31**, 547–550.

Li, Z., and Z.-W. Yan, 2009: Homogenized daily mean/maximum/minimum temperature series for China from 1960–2008. *Atmos. Oceanic Sci. Lett.*, **2**, 237–243, https://doi.org/10.1080/16742834.2009.11446802.

——, L. Cao, Y. Zhu, and Z. Yan, 2016: Comparing two homogenized datasets of daily maximum/mean/minimum temperatures in China during 1960–2013. *J. Meteor. Res.*, **30**, 53–66, https://doi.org/10.1007/s13351-016-5054-x.

Liebmann, B., and C. A. Smith, 1996: Description of a complete (interpolated) outgoing longwave radiation dataset. *Bull. Amer. Meteor. Soc.*, **77**, 1275–1277.

Liu, Y., Z. Cheng, A. Cai, and M. Ye, 2008: Diagnostic analysis of long-endurance high temperature event in Guangdong province in July 2007 (in Chinese). *Meteor. Sci. Technol.*, **32**, 734–739.

Livezey, R., and W. Chen, 1983: Statistic field significance and its determination by Monte Carlo techniques. *Mon. Wea. Rev.*, **111**, 46–59, https://doi.org/10.1175/1520-0493(1983)111<0046:SFSAID>2.0.CO;2.

Mao, J., and J. Chan, 2005: Intraseasonal variability of the South China Sea summer monsoon. *J. Climate*, **18**, 2388–2402, https://doi.org/10.1175/JCLI3395.1.

Rayner, N., D. E. Parker, E. B. Horton, C. K. Folland, L. V. Alexander, D. P. Rowell, E. C. Kent, and A. Kaplan, 2003: Global analyses of sea surface temperature, sea ice, and night marine air temperature since the late nineteenth century. *J. Geophys. Res.*, **108**, 1063–1082, https://doi.org/10.1029/2002JD002670.

Ren, B., and R. Huang, 2002: 10–25-day intraseasonal variations of convection and circulation associated with thermal state of the western Pacific warm pool during boreal summer.

Adv. Atmos. Sci., **19**, 321–336, https://doi.org/10.1007/s00376-002-0025-9.

Teofilo, L.-C., and J. T. Stitt, 1995: Heatstroke and other heat-related illnesses. The maladies of summer. *Postgrad. Med.*, **98**, 26–36.

UNDP, 2016: Climate change and labour: Impacts of heat in the workplace. United Nations Development Programme, 33 pp., http://admin.indiaenvironmentportal.org.in/files/file/Climate-Change-and-Labour-Impacts-Of-Heat-In-The-Workplace.pdf.

Valor, E., V. Meneu, and V. Caselles, 2001: Daily air temperature and electricity load in Spain. *J. Appl. Meteor.*, **40**, 1413–1421, https://doi.org/10.1175/1520-0450(2001)040<1413:DATAEL>2.0.CO;2.

Wang, B., R. Wu, and X. Fu, 2000: Pacific–East Asian teleconnection: How does ENSO affect East Asian climate? *J. Climate*, **13**, 1517–1536, https://doi.org/10.1175/1520-0442(2000)013<1517:PEATHD>2.0.CO;2.

Wang, W., W. Zhou, and D. Chen, 2014: Summer high temperature extremes in southeast China: Bonding with the El Niño–Southern oscillation and East Asian summer monsoon coupled system. *J. Climate*, **27**, 4122–4138, https://doi.org/10.1175/JCLI-D-13-00545.1.

——, ——, X. Li, W. Xin, and D. Wang, 2016: Synoptic-scale characteristics and atmospheric controls of summer heat waves in China. *Climate Dyn.*, **46**, 2923–2941, https://doi.org/10.1007/s00382-015-2741-8.

Wang, Y., P. Zhai, and H. Tian, 2006: Extreme high temperatures in southern China in 2003 under the background of climate change (in Chinese). *Meteor. Mon.*, **32**, 27–33.

Wei, K., and W. Chen, 2009: Climatology and trend of high temperature extremes across China in summer. *Atmos. Ocean. Sci. Lett.*, **2**, 153–158, https://doi.org/10.1080/16742834.2009.11446795.

——, and ——, 2011: An abrupt increase in the summer high temperature extreme days across China in the mid-1990s. *Adv. Atmos. Sci.*, **28**, 1023–1029, https://doi.org/10.1007/s00376-010-0080-6.

Wei, J., H. Yang, and S. Sun, 2004: Relationship between the anomaly longitudinal position of subtropical high in the western Pacific and severe hot weather in North China in summer (in Chinese). *Acta Meteor. Sin.*, **62**, 308–316.

Wilks, D., 2006: Hypothesis testing. *Statistical Methods in the Atmospheric Sciences*, International Geophysics Series, Vol. 91, Academic Press, 131–177.

WMO, 2013: *The Global Climate 2001–2010, A Decade of Climate Extremes*. WMO-1103, 110 pp.

——, 2015: Provisional statement on the status of global climate in 2011–2015. World Meteorological Organization, 13 pp., https://www.wmo.int/pages/meetings/documents/WMO2011-2015.final_-1.pdf.

Wu, B., T. Li, and T. Zhou, 2010: Relative contributions of the Indian Ocean and local SST anomalies to the maintenance of the western North Pacific anomalous anticyclone during the El Niño decaying summer. *J. Climate*, **23**, 2974–2986, https://doi.org/10.1175/2010JCLI3300.1.

Xie, S.-P., K. Hu, J. Hafner, H. Tokinaga, Y. Du, G. Huang, and T. Sampe, 2009: Indian Ocean capacitor effect on Indo–western Pacific climate during the summer following El Niño. *J. Climate*, **22**, 730–747, https://doi.org/10.1175/2008JCLI2544.1.

Xu, K., and R. Lu, 2015: Break of the western North Pacific summer monsoon in early August. *J. Climate*, **28**, 3420–3434, https://doi.org/10.1175/JCLI-D-14-00588.1.

Yang, H., and C.-Y. Li, 2005: Diagnostic study of serious high temperature over South China in 2003 summer (in Chinese). *Climatic Environ. Res.*, **10**, 80–85.

Zhang, Y., and S. Zhang, 2010: Causation analysis on a large-scale continuous high temperature process occurring in North China plain (in Chinese). *Meteor. Mon.*, **36**, 8–13.